

Article

# The Application of Electrical Parameters to Reflect the Hydration Process of Cement Paste with Rice Husk Ash

Hui Wang <sup>1,\*</sup>, Lingxuan Hu <sup>2</sup>, Peng Cao <sup>3</sup>, Baoxin Luo <sup>1</sup>, Jing Tang <sup>1</sup>, Feiting Shi <sup>4,\*</sup>, Jinyan Yu <sup>1</sup>, Hongjie Li <sup>1</sup> and Kaikai Jin <sup>1</sup>

<sup>1</sup> School of Civil and Environmental Engineering, Ningbo University, Ningbo 315000, China

<sup>2</sup> School of Civil Engineering, Harbin Institute of Technology, Harbin 150090, China

<sup>3</sup> College of Architecture and Civil Engineering, Beijing University of Technology, Beijing 100124, China

<sup>4</sup> Civil Engineering Department, Yancheng Institute of Technology, Yancheng 224051, China

\* Correspondence: wanghui4@nbu.edu.cn (H.W.); shifeiting@ycit.cn (F.S.)

Received: 1 July 2019; Accepted: 27 August 2019; Published: 2 September 2019



**Abstract:** This paper aims to study the electrical parameters (electrical resistivity and alternating current (AC) impedance spectroscopy) of cement paste with rice husk ash (RHA). The water to cement (Mass ratio of water to cement (w/c)) ratios of the paste in this study varied from 0.4 to 0.5. The mass ratio of rice husk ash in each w/c ratio of specimens ranged from 0% to 15% by mass of cement. Scanning electron microscopy (SEM) and X-ray diffraction (XRD) were used to determine the microstructures of specimens. Moreover, the slump flow and plastic viscosity of fresh paste were determined. The results indicated that with the increasing dosage of RHA, the fluidity decreased, while the plastic viscosity increased. Meanwhile, a high w/c ratio led to a low plastic viscosity and high slump flow. The electrical resistivity of RHA cement paste gradually ascended with the increasing curing period. The conduction of specimens intricately changed by mixing RHA, a reasonable equivalent circuit was selected to describe the conduction mechanism by AC impedance spectroscopy. Additionally, the results of XRD and SEM showed that RHA could effectively promote the hydration process as well as decrease the size and number of cracks in hardened cement paste.

**Keywords:** electrical resistivity; AC impedance spectroscopy; cement paste; rice husk ash; equivalent circuit

## 1. Introduction

Rice husk ash (RHA) is produced from agricultural waste (rice husk) [1–4]. The main component of RHA contains a large amount of amorphous silica. Therefore, like silica fume, RHA is a kind of active mineral admixture [5]. Zhuang et al. pointed out that RHA is effective to decrease the porosity and  $\text{Ca}(\text{OH})_2$  in cement paste [6]. Moreover, as described in some literatures, RHA possesses a very high pozzolanic reactivity comparable with that of silica fume (SF) [7–9]. RHA has been proven by scholars to replace silica fume for achieving high strength/performance concrete [10,11].

Van et al. reported that the addition of RHA can reduce free water in high strength/performance concrete, thus improving its mechanical properties [12]. Additionally, RHA is able to decrease the pore size and numbers in concrete, thus enhancing the compressive strength and impermeability [13]. Moreover, RHA was considered as an internal curing agent to decrease autogenous shrinkage [14]. However, RHA may decrease the fluidity of fresh concrete. The influences of RHA on the rheological properties of fresh concrete and the rheological mechanism were unknown.

The hydration of cement material is a complicated physical and chemical process [15]. This process controls the microstructure and macro performance of cement matrix [16]. Many literatures on studying

hydration mechanism have been published [17]. Generally, some researchers analyzed the hydration and hardening mechanisms by means of scanning electron microscopy (SEM), X-ray diffraction (XRD), and Fourier transform infrared spectroscopy (FT-IR) [18,19]. It is known that continuous monitoring of hydration process information may not be obtained from the above methods. In addition, the preparation environment when drying samples for microscopy observations and analysis to characterize hydration process will also affect the test results. Aiming at these problems, some scholars have begun to focus on nondestructive testing methods, electrical testing methods, microwave energy methods, and ultrasound detection methods. These methods are the most commonly used testing methods [20–22]. Compared with the methods mentioned above, nondestructive testing (NDT) is undoubtedly a better way to analyze the complex hydration process of cement materials.

Recently, electrical properties of cement-based materials were determined to reflect the service performance of concrete, e.g., the hydration process etc. Wang et al. pointed out that cement mortar with carbon nanofibers was able to sense freeze-thaw damage of materials, environmental temperatures, applied stress, strain etc. by sensing the evolution of the specimen's electrical resistivity [23]. The self-sensing cement composite with conductive fibers is called intrinsic self-sensing concrete [24]. Moreover, Han et al. found that the electrochemical impedance spectroscopy (EIS) and equivalent circuits are able to analyze the conductive mechanisms of cement-based composite with conductive fillers [25]. However, few researchers focus on the conductive performance of plain RHA cement paste with different rheological properties and curing ages. Obviously, little attention was paid to electrical properties of cement-based materials that reflected the hydration process of RHA cement matrix [26].

This paper studies the influence of rice husk ash content and curing ages on the rheological properties (slump flow and plastic viscosity) and electrical parameters (electrical resistance and alternating current (AC) impedance spectroscopy) of cement paste. Mass ratio of RHA varied from 0% to 15% by the total mass of bind materials. In this research, water-cement (w/c) ratios were 0.4, 0.45, and 0.5. SEM technology has greatly helped to elucidate the microstructures, and the XRD method was applied to determine the composition of specimens with RHA.

## 2. Experiment

### 2.1. Raw Materials

The 42.5 ordinary Portland cement (P.O 42.5) provided by Yancheng Conch Cement Co., Ltd. (Yancheng, China) was used as the binder material in this research. The fluidity of fresh paste was adjusted by a polycarboxylate-based, high-range water-reducing agent. The RHA was fabricated by burning origin rice husk in an airtight high temperature furnace. The furnace filled with rice husk was first heated at a rate of 10 °C to 500 °C for 2 h, and then the calcined residue was ground in a vibrating mill for 15 min. The particle size distribution and chemical compound were the same as in Reference [27]. The particle passing percentage and chemical composition of cement and RHA are shown in Tables 1 and 2. In Table 2, "R<sub>2</sub>O" means "Na<sub>2</sub>O + K<sub>2</sub>O". The particle passing percentage of cementitious materials was provided by Yancheng Conch Cement Co., Ltd. The method for testing the particle passing percentage of cementitious materials was obtained according to the testing method for the particle size of cement. Additionally, the chemical composition of cement and RHA were chosen in a previous study [27].

**Table 1.** Particle passing percentage of the cementitious materials.

Particle Size/ $\mu\text{m}$ Types	0.3	0.6	1	4	8	16	32	64
Cement (P.O 42.5)	0	0.33	2.66	15.01	28.77	46.64	72.73	93.59
RHA	0	0.58	6.84	18.32	32.14	51.62	78.45	96.32

**Table 2.** Chemical composition of the cementitious materials.

Types	Chemical Composition/%								
	SiO <sub>2</sub>	Al <sub>2</sub> O <sub>3</sub>	Fe <sub>2</sub> O <sub>3</sub>	MgO	CaO	SO <sub>3</sub>	R <sub>2</sub> O	MnO	H <sub>2</sub> O
Cement (P.O 42.5)	20.86	5.47	3.94	1.73	62.23	2.66	0.48	0	0
RHA	91.56	0.19	0.17	0.65	1.07	0.47	3.92	0.74	0.23

### 2.2. Mixing Proportion

Table 3 shows the mixing proportions of all groups of the paste. In this experiment, the w/c ratios were 0.4, 0.45, and 0.5. In each group of specimens, the dosage of RHA varied from 0% to 15%.

**Table 3.** Mixing proportion of fresh cement paste.

Samples	Cement	Water	RHA	Water Reducing Agent
RHA-1	100	40	0	0.6
RHA-2	95	40	5	0.6
RHA-3	90	40	10	0.6
RHA-4	85	40	15	0.6
RHA-5	100	45	0	0.6
RHA-6	95	45	5	0.6
RHA-7	90	45	10	0.6
RHA-8	85	45	15	0.6
RHA-9	100	50	0	0.6
RHA-10	95	50	5	0.6
RHA-11	90	50	10	0.6
RHA-12	85	50	15	0.6

### 2.3. Specimens Preparation and Measurement

Cement and water were mixed uniformly in the NJ-160A cement paste mixer and stirred at a speed of 140 rpm for 2 min. Next, the mixture was mixed again at a speed of around 285 rpm for another 2 min. After that, the slump flow of the prepared fresh paste was measured by using a steel cone with a bottom diameter of 60 mm, a top diameter of 36 mm and a height of 60 mm. Additionally, an NXS-11B rotating viscometer manufactured by Chengdu Leadership Instruments Co., Ltd. (Chengdu, China) was used to determine the plastic viscosity of the paste. To measure the electrical resistance, specimens with a size of 20 mm × 30 mm × 35 mm were fabricated and then the electrical resistances were tested by a TH2810D LCR digital electric bridge (Changzhou Tonghui Co., Ltd., Changzhou, China) with a frequency ranging from 100 Hz to 10 kHz. The tests were conducted at an AC voltage of 1 V and frequency of 10 kHz with the embedded two-pole layout method, as shown in Figure 1a. The electrodes were made of corrosion resistant AISI 316L stainless steel mesh with a size of 2.0 cm × 3.5 cm and a thickness of 0.8 mm. The AC electrical resistance along the longitudinal axis direction of the cube was determined. Three specimens were measured for each group. The electrochemical impedance spectroscopy was tested by an electrochemical workstation (Shanghai Chen Hua Instrument Co., LTD, Shanghai, China) as shown in Figure 1b. The microstructure and crystal types of hydration products were determined by JSM-6360LV scanning electron microscope (Japan electron optics laboratory, Tokyo, Japan) and D8 ADVANCE X-ray diffractometer (Bruker Corp., Tokyo, Japan) respectively. Before the experiments, the samples were dried in a vacuum drying oven (Shanghai Yi Heng Instrument Co., LTD DZF-6020, Shanghai, China) at 60 °C. When SEM observations were carried out all samples were metallized with gold.

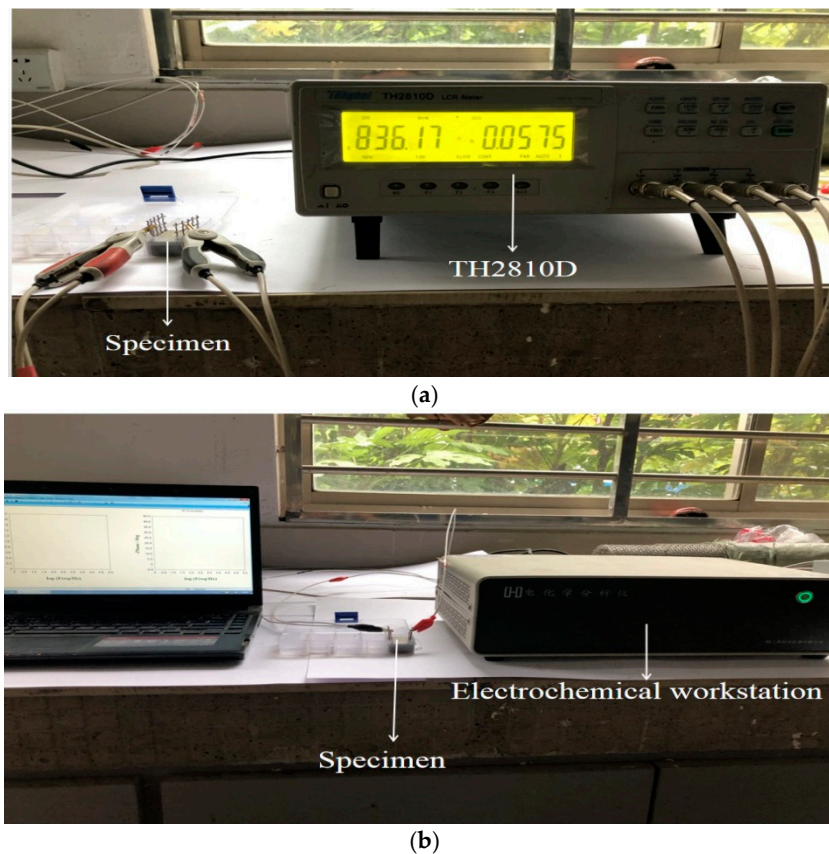


**Figure 1.** Electrical parameters measurement: (a) Electrical resistance measurement; (b) Alternating current (AC) impedance spectroscopy.

### 3. Results and Discussion

#### 3.1. Rheological Performance of Cement Paste

Figure 2 shows the variation of slump flow and plastic viscosity with the increasing dosage of RHA. The shear rate for plastic viscosity determination was 8 rpm. As shown in Figure 2, more RHA resulted in a lower slump flow and higher plastic viscosity. Moreover, higher w/c ratios presented higher slump flow and lower plastic viscosity. The increasing content of RHA decreased the slump flow and increased plastic viscosity because the incorporation of RHA could adsorb some free water in fresh paste that had resulted in decreasing the fluidity and increasing the viscosity of fresh paste [12]. However, higher w/c ratios led to higher fluidity and lower viscosity, this was attributed to the fact that cement paste with higher w/c ratios contains more free water, therefore the flowing property was improved, and the viscosity was decreased by higher w/c ratios [28].

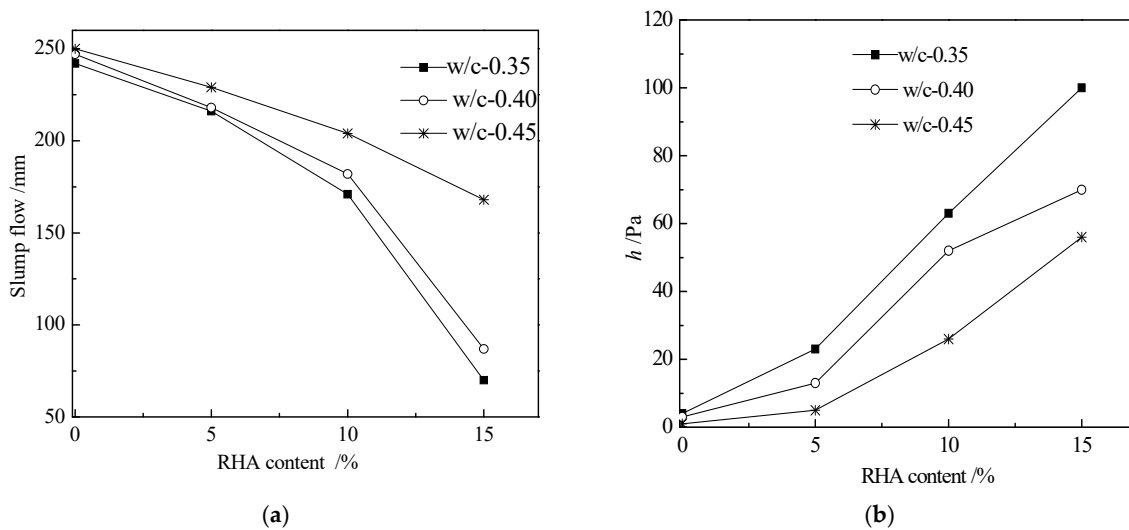


**Figure 2.** Slump flow and viscosity of fresh paste with different dosage of Rice husk ash (RHA): (a) Slump flow; (b) Viscosity.

### 3.2. Electrical Resistivity

Figures 3–5 show the electrical resistivity of specimens with RHA content ranging from 0% to 15%. As shown in Figures 3–5, the resistivity of all specimens increased with the increasing curing time because the increasing hydration of the cement paste might decrease the free conductive ions in the cement paste thus resulting in decreasing the conductivity [28–31]. Therefore, the resistivity of specimens increased with increasing curing ages. At the curing ages from 3 h to 24 h, the electrical resistivity of the cement paste with RHA from 0% to 10% linearly increased with the curing ages. However, for the specimens with 15% RHA content, the electrical resistivity of all specimens rarely changed with the curing ages. Moreover, the electrical resistivity of specimens with w/c ratios of 0.4 and 0.45 decreased slightly with RHA content. This might be attributed to the fact that RHA is a pozzolanic material, hence, the portlandite first formed and then reacted with RHA, and thus the setting time and hardening were delayed with the increase in RHA content [21]. However, when the curing ages ranged from 336 h to 672 h, the electrical resistivity of specimens with w/c ratios of 0.4 and 0.45 increased slightly with RHA content, because RHA is effective to diminish conductive free ions by accelerating hydration and decreasing the fluidity of fresh paste. Above all, the conductive performance of specimens with RHA is a complex process. The addition of RHA was effective to decrease the fluidity of the fresh paste and reduce the free water in the cement paste, thus decreasing the conductive ions of pore solution and increasing the resistivity of specimens. The retarding action of RHA in cement paste might decrease the resistivity of specimens [21]. In this study, w/c ratios had little influence on the resistivity of specimens. This might be attributed to some complicated reasons that will be studied in the future.

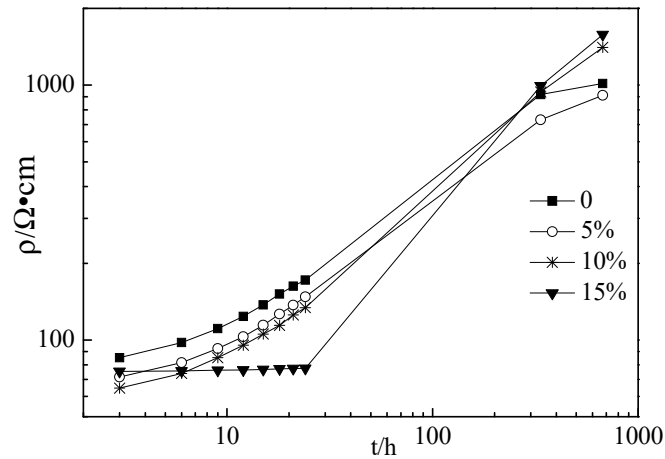


Figure 3. Electrical resistivity of specimens with w/c ratio of 0.40.

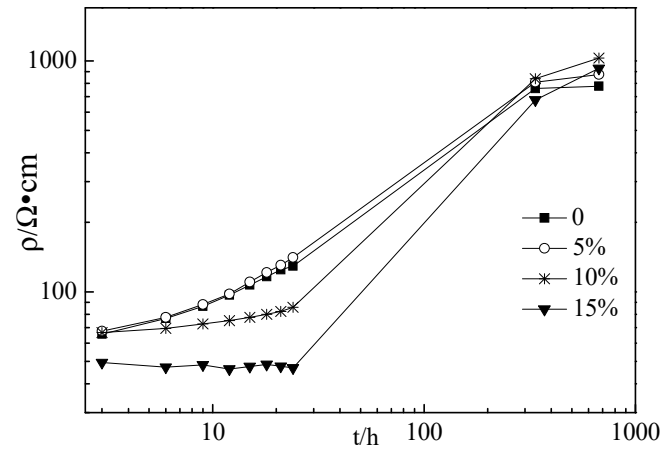


Figure 4. Electrical resistivity of specimens with the w/c ratio of 0.45.

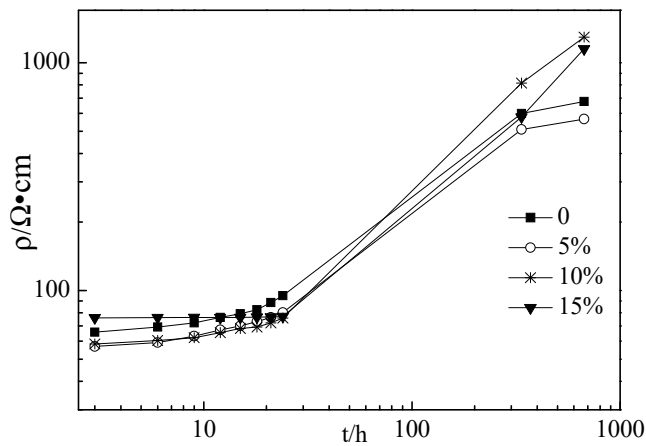


Figure 5. Electrical resistivity of specimens with the w/c ratio of 0.50.

### 3.3. Electrochemical Impedance Spectroscopy (EIS)

The electrical resistances of the cement paste with different w/c ratios are shown in Figures 6–8. EIS and corresponding equivalent circuits were used to analyze the mechanism of conductive properties. The imaginary and real components of the electrochemical impedance spectroscopy represent the electrical reactance and resistance, respectively [25]. It can be seen that the imaginary and real

components of all groups increase linearly with real components as frequency decreases from left to right. The Chi-squared is less than or equal to  $2.053 \times 10^{-3}$ . This verifies that the selected equivalent circuits are reasonable for describing the conductive pathways in Figures 6–8. When the water to cement ratio (Mass ratio of water to cement) was 0.40, the growth rate of imaginary components with real components was accelerated by the increased curing ages. However, when the water cement ratios were 0.45 and 0.50, the growth rates of the imaginary and real components were random. The internal causes will be studied in the future. Meanwhile, as shown in Figures 6–8, the increase of the curing ages was effective to increase the real components, which meant that the electrical resistances of specimens increased as well. The incorporation of RHA can decrease the real components at the initial curing ages (3–24 h) but increase the real components at the long-term curing ages (1–28 d). This behavior was described and analyzed in Part 3.2.

Figure 9 shows the corresponding equivalent circuits of specimens with RHA. The circular section can be represented by the parallel of resistance and capacitance elements. The initial resistance ( $R_s$ ) corresponds to the contact resistance between specimen and electrodes. Then, the following series connected electrical components represented shunt-wound resistance ( $R_1$ ) and electrical capacitance ( $C_1$ ) of the pore solution. A conductive pathway was formed by the pore solution in the cement matrix. The addition of RHA can decrease the fluidity and enhance the hydration thus blocking the conductive channels in specimens. Moreover, due to the electrical capacitances of specimens, the specimens present strong zero drift phenomena in the electrical performance.

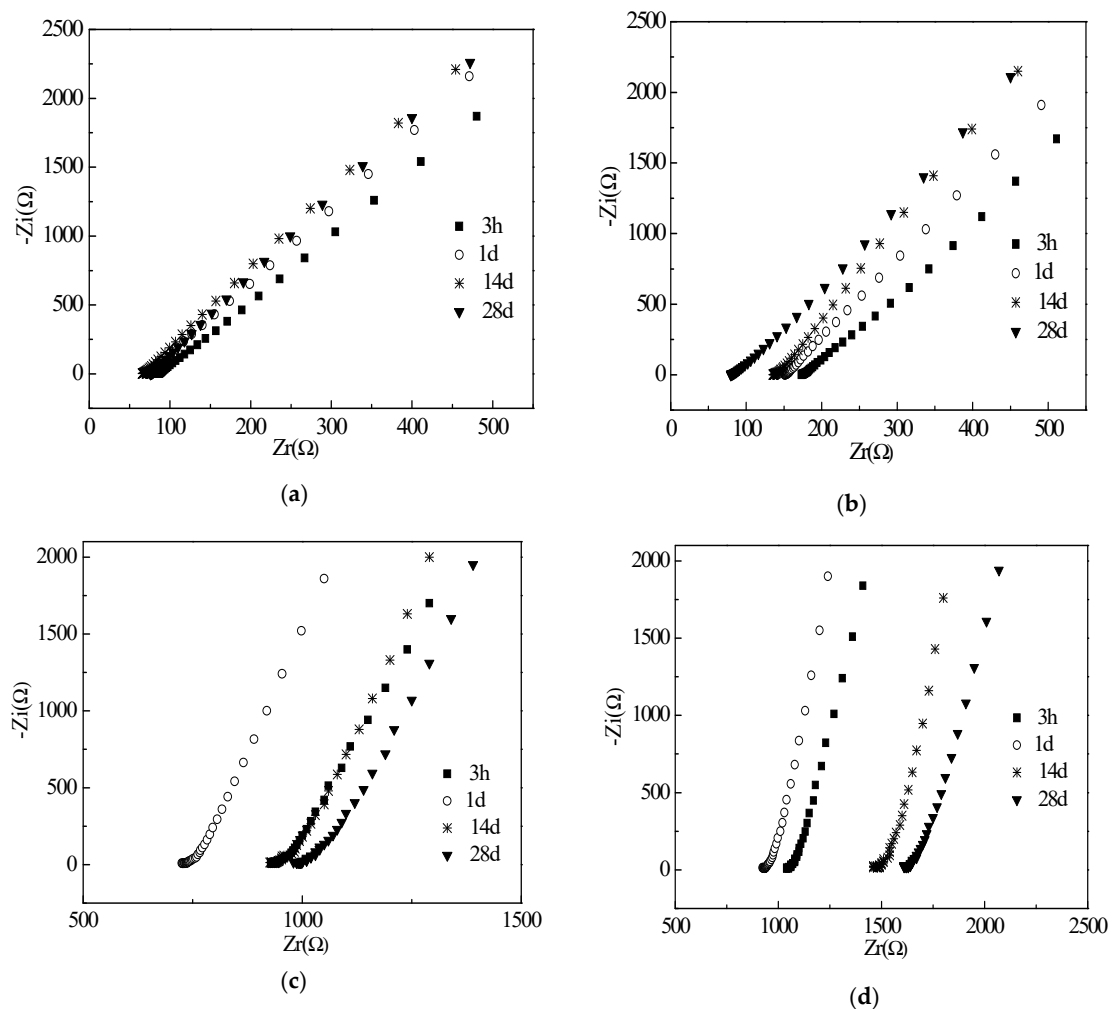


**Figure 6.** Electrochemical impedance spectroscopy (EIS) curves of specimens with w/c ratio of 0.40: (a) RHA-1; (b) RHA-2; (c) RHA-3; (d) RHA-4.

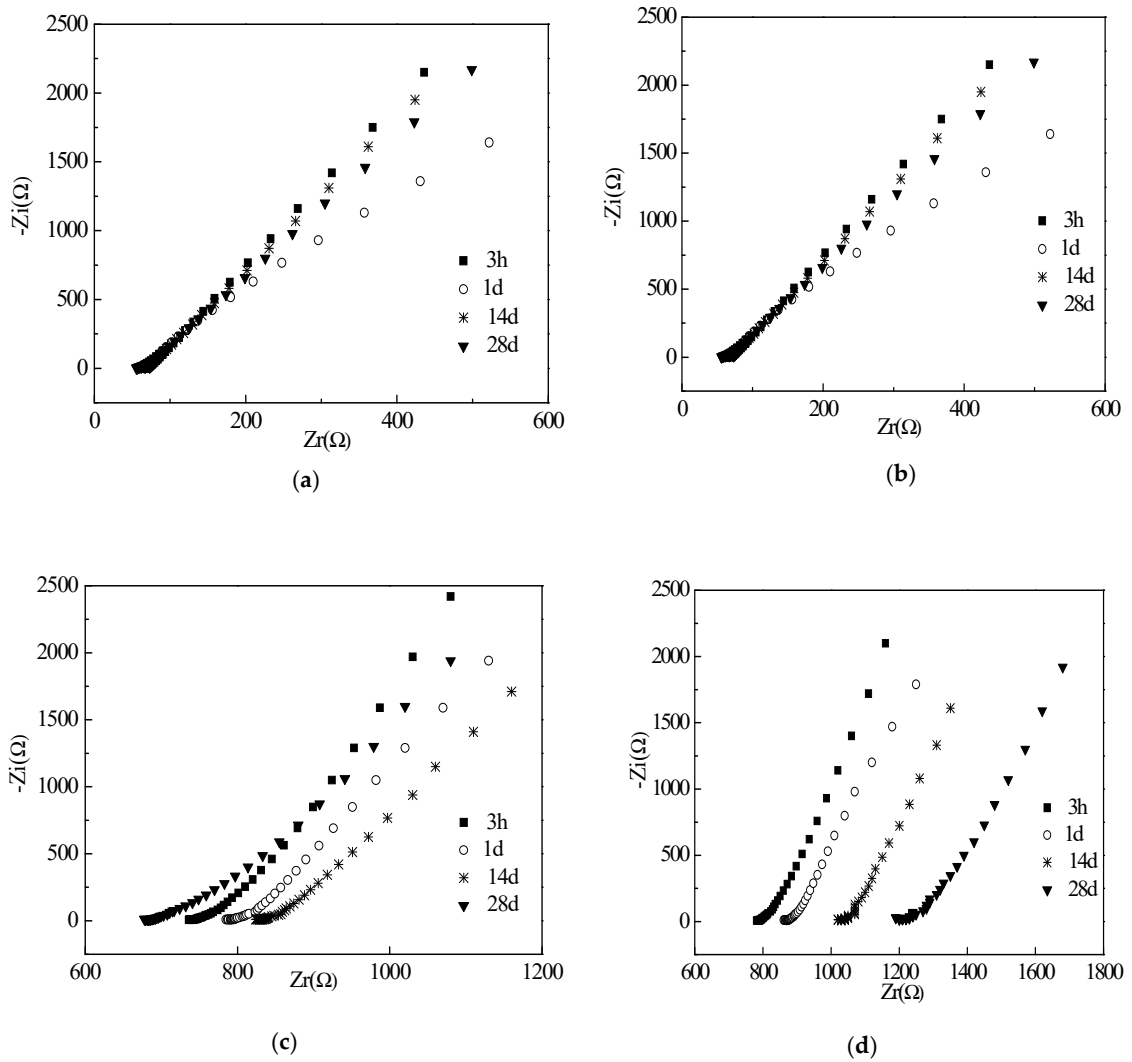


Figure 7. EIS curves of specimens with w/c ratio of 0.45: (a) RHA-5; (b) RHA-6; (c) RHA-7; (d) RHA-8.

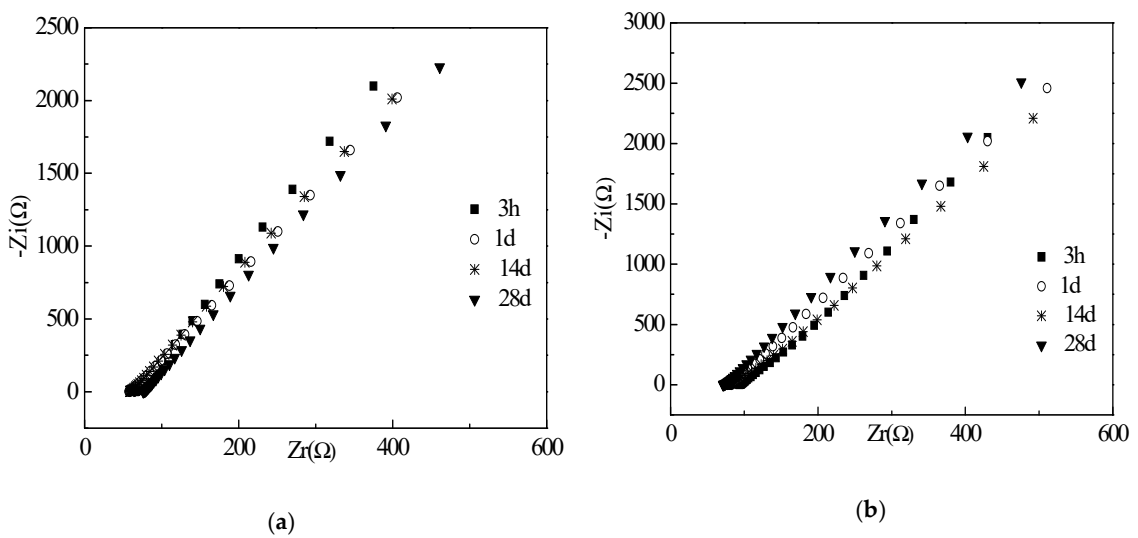


Figure 8. Cont.

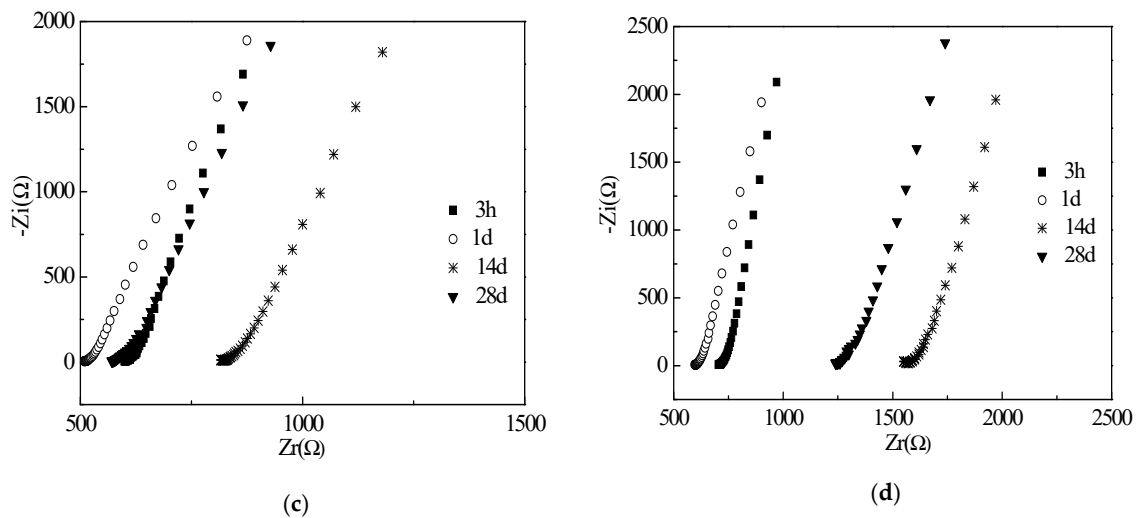


Figure 8. EIS curves of specimens with w/c ratio of 0.50: (a) RHA-10; (b) RHA-11; (c) RHA-12; (d) RHA-12.

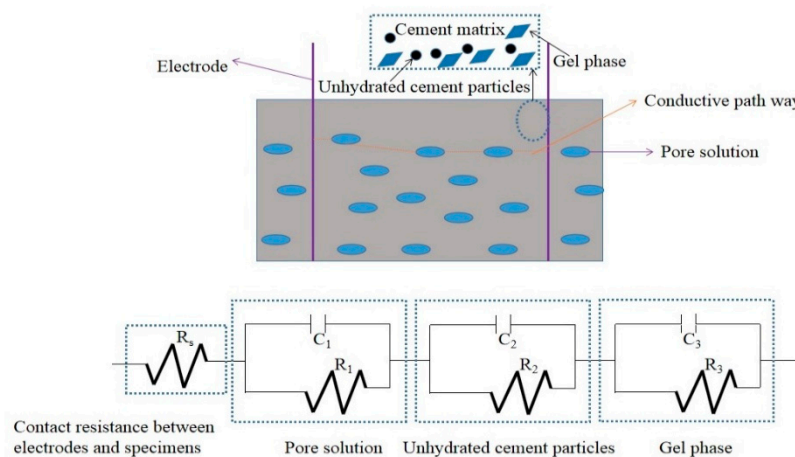
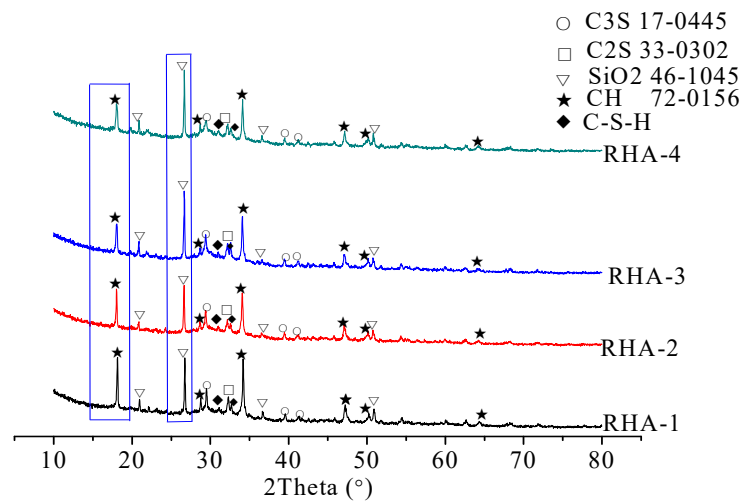


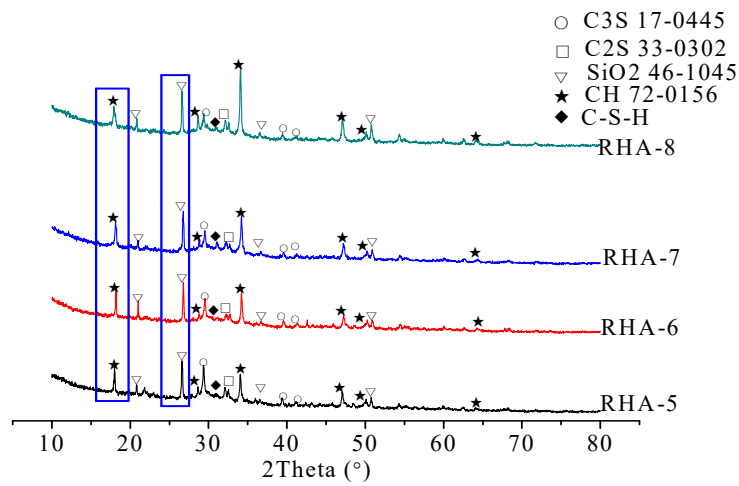
Figure 9. Corresponding equivalent circuits of specimens with RHA.

### 3.4. Microscopic Analysis

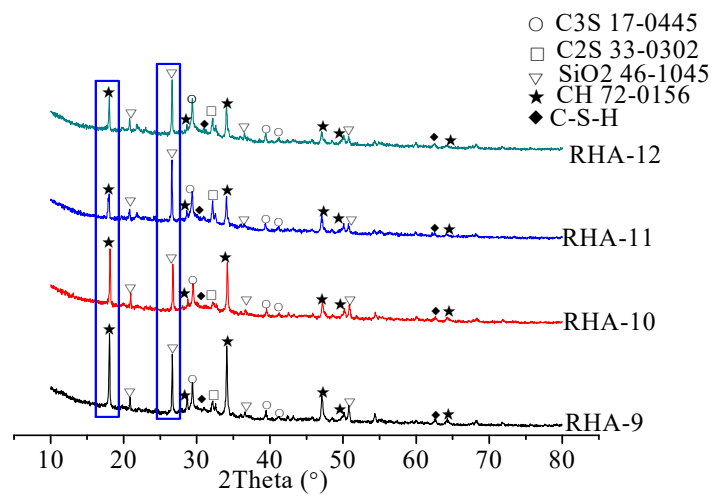
Figure 10 shows the XRD patterns of specimens after a 28-day standard curing. From Figure 10 it can be seen that the diffraction peaks of  $3\text{CaO}\cdot\text{SiO}_2$  ( $\text{C}_3\text{S}$ ),  $2\text{CaO}\cdot\text{SiO}_2$  ( $\text{C}_2\text{S}$ ), and  $\text{SiO}_2$  are significantly strong, which indicates good crystallinity [32,33]. Results indicated that all specimens were mainly constituted of unhydrated cement particles such as  $3\text{CaO}\cdot\text{SiO}_2$  ( $\text{C}_3\text{S}$ ),  $2\text{CaO}\cdot\text{SiO}_2$  ( $\text{C}_2\text{S}$ ),  $\text{SiO}_2$ , and hydration products like calcium hydroxide (CH) and hydrated calcium silicate (C-S-H). Figure 10 shows that the height of diffraction peaks of  $\text{SiO}_2$  increased with the increase of RHA, whereas the height of diffraction peaks of CH and  $\text{C}_3\text{S}$  decreased with the increase of RHA. These results can be attributed to the high RHA content leading to a low fraction of  $\text{SiO}_2$  in the cement paste. Moreover, the increasing dosage of RHA might have accelerated the hydration process of the cement paste, which led to the decrease of CH and  $\text{C}_3\text{S}$  [17–19].



(a)



(b)



(c)

**Figure 10.** XRD spectra of specimens with RHA: (a) w/c ratio of 0.40; (b) w/c ratio of 0.45; (c) w/c ratio of 0.50.

Figure 11 shows the scanning electron microscope (SEM) photos of specimens. The curing ages of all specimens were 28 days. As shown in Figure 11,  $\text{Ca}(\text{OH})_2$  crystals can be observed obviously when RHA is not added to the paste. Many flocky hydration products exist in specimens when they contain RHA. Moreover, cracks in specimens decreased with the increasing dosage of RHA. Additionally, the decreasing w/c ratios led to reduce the numbers and size of crack in specimens. Results indicate that RHA was effective to improve the compactness and decrease the cracks in specimens. Previous research pointed out that the amorphous silica in RHA reacted with calcium hydroxide forming C-S-H. Moreover, as described in Sensale's research, the particle size of RHA was less than  $45\ \mu\text{m}$ , as being the nucleation point due to hydration products [34]. Therefore, RHA was able to improve the compactness of the cement paste.

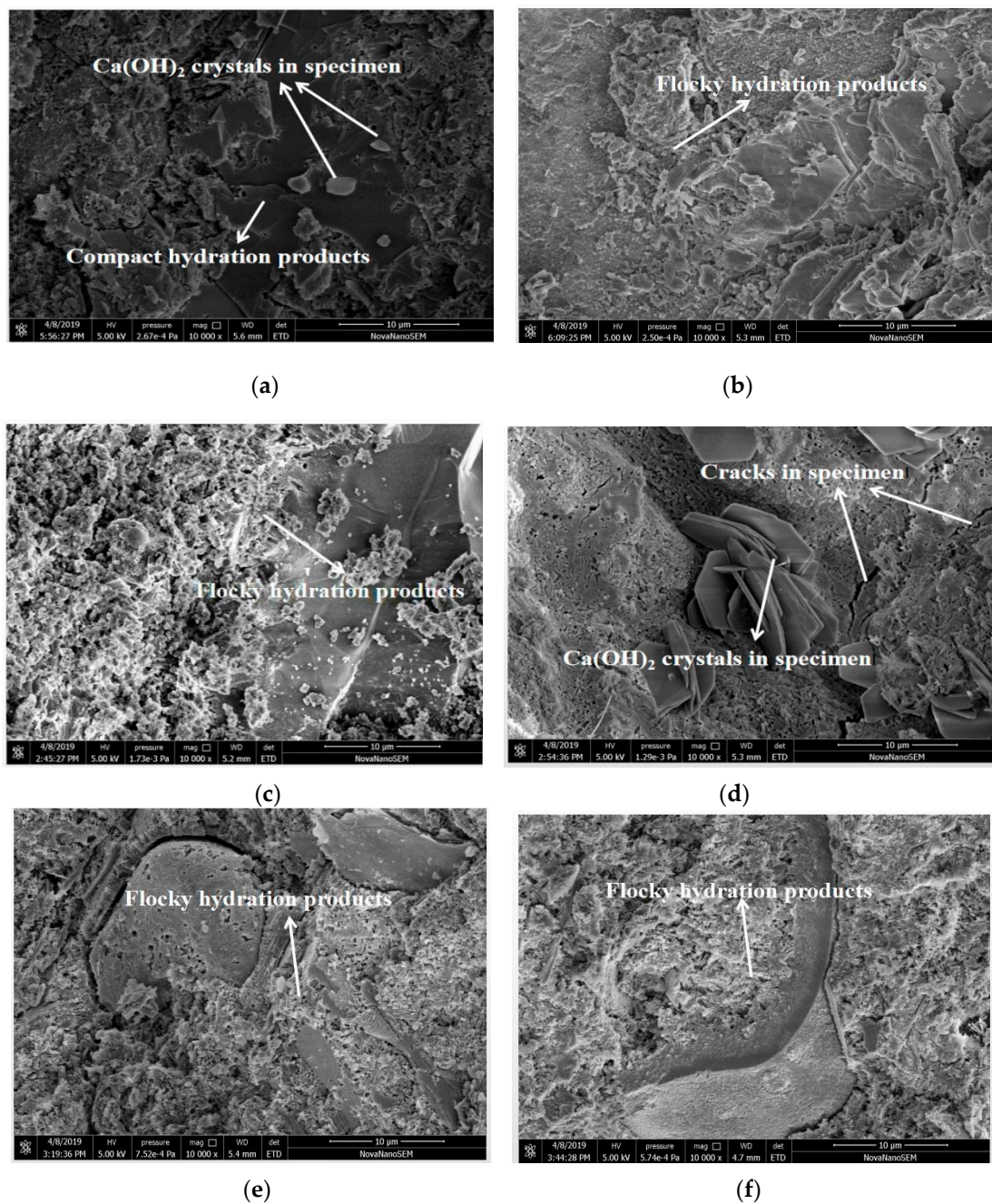
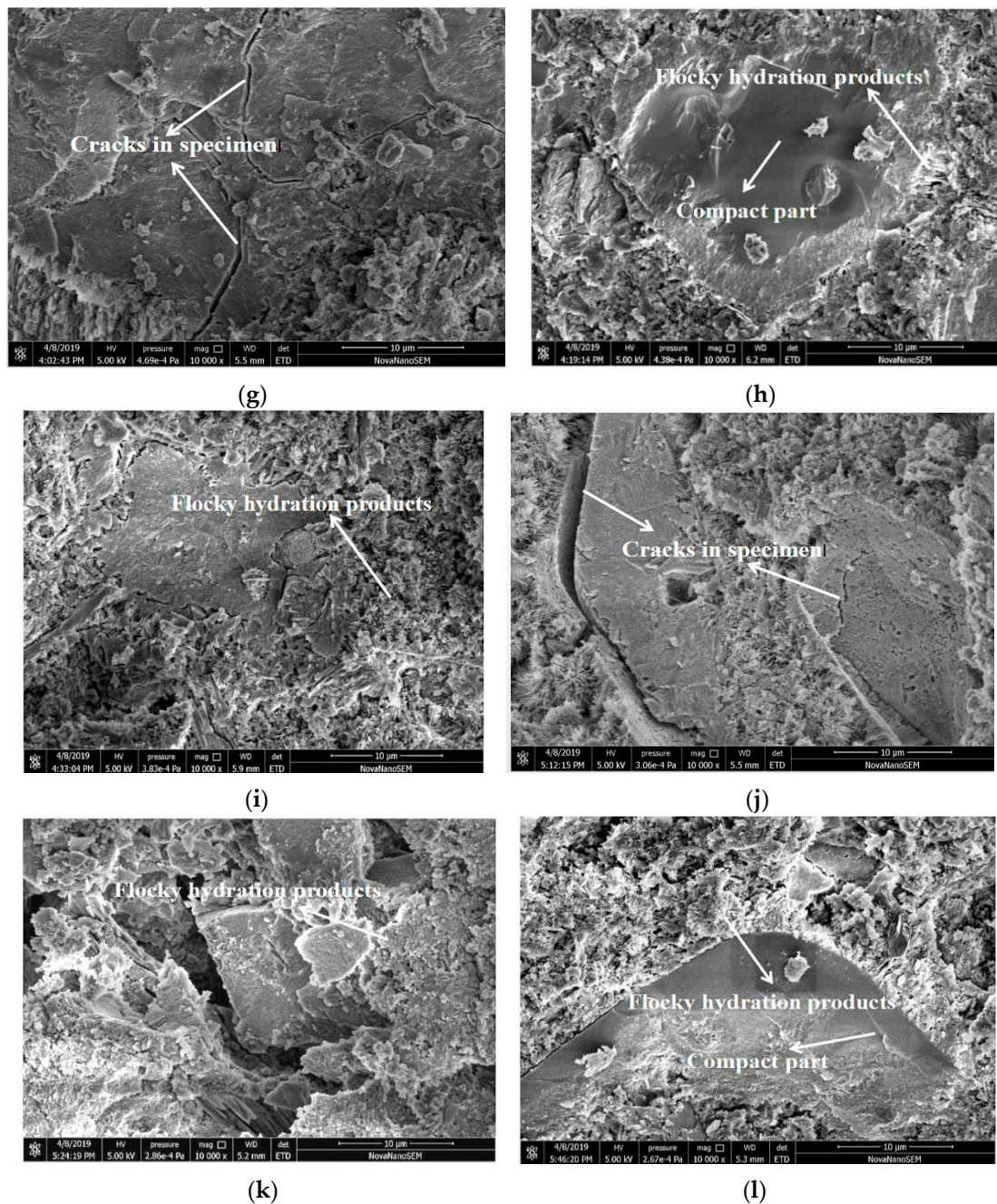


Figure 11. Cont.



**Figure 11.** SEM micrographs of specimens with RHA: (a) RHA-1 (10000); (b) RHA-2 (10000); (c) RHA-3 (10000); (d) RHA-4 (10000); (e) RHA-5 (10000); (f) RHA-6 (10000); (g) RHA-7(10000); (h) RHA-8 (10000); (i) RHA-9 (10000); (j) RHA-10 (10000); (k) RHA-11 (10000); (l) RHA-12 (10000).

#### 4. Conclusions

Based on this study, the following conclusions can be drawn.

- (1) The slump flow of fresh cement paste was reduced, and the plastic viscosity was increased by the increasing addition of RHA and lower w/c ratios.
- (2) The resistivity of all specimens increased with the increasing curing ages. The addition of RHA had a complex influence on the conduction of specimens, due to its influence on the number of electrical free ions and the retarding action in cement paste. The equivalent circuits consisted of three resistor elements and three capacitance elements. Resistors or capacitances were in

series connection respectively. A parallel circuit was more reasonable between each capacitance and resistor.

- (3) RHA was effective to improve the compactness of the cement paste. Moreover, the hydration products (CH) were decreased by the increasing addition of RHA.

**Author Contributions:** Investigation, Writing—Original Draft Preparation, Visualization, Software, Resources, Project Administration and Funding Acquisition, H.W.; Investigation, Data Curation and Formal Analysis, L.H., P.C. and B.L.; Writing—Review and Editing, F.S.; Supervision and Methodology, J.Y., H.L. and K.J.

**Funding:** This study was sponsored by the K.C. Wong Magna Fund in Ningbo University, National Natural Science Foundation of China [No.51808300], Science and Technology Projects of the Ministry of Housing and Urban Rural Development of China [No. 2018-K9-024; No. 2018-K9-054], Natural Science Foundation of Ningbo [No. 2018A610357], and School Research Fund of Ningbo University [No. XYL19010].

**Conflicts of Interest:** The authors declare no conflict of interest.

## References

1. Mikulčić, H.; Klemeš, J.; Vujanović, M.; Urbaniec, K.; Duić, N. Reducing greenhouse gasses emissions by fostering the deployment of alternative raw materials and energy sources in the cleaner cement manufacturing process. *J. Clean. Prod.* **2016**, *136*, 119–132. [[CrossRef](#)]
2. Schneider, M.; Romer, M.; Tschudin, M.; Bolio, H. Sustainable cement production—Present and future. *Cem. Concr. Res.* **2011**, *41*, 642–650. [[CrossRef](#)]
3. Damtoft, J.; Lukasik, J.; Herfort, D.; Sorrentino, D.; Gartner, E.; Gartner, E. Sustainable development and climate change initiatives. *Cem. Concr. Res.* **2008**, *38*, 115–127. [[CrossRef](#)]
4. Flatt, R.J.; Roussel, N.; Cheeseman, C.R. Concrete: An eco material that needs to be improved. *J. Eur. Ceram. Soc.* **2012**, *32*, 2787–2798. [[CrossRef](#)]
5. Duxson, P.; Provis, J.L. Designing Precursors for Geopolymer Cements. *J. Am. Ceram. Soc.* **2008**, *91*, 3864–3869. [[CrossRef](#)]
6. Zhuang, X.Y.; Chen, L.; Komarneni, S.; Zhou, C.H.; Tong, D.S.; Yang, H.M.; Yu, W.H.; Wang, H. Fly ash-based geopolymer: Clean production, properties and applications. *J. Clean. Prod.* **2016**, *125*, 253–267. [[CrossRef](#)]
7. Van, V.-T.-A.; Rößler, C.; Bui, D.-D.; Ludwig, H.-M. Mesoporous structure and pozzolanic reactivity of rice husk ash in cementitious system. *Constr. Build. Mater.* **2013**, *43*, 208–216. [[CrossRef](#)]
8. Chandrasekhar, S.; Satyanarayana, K.G.; Pramada, P.N.; Raghavan, P.; Gupta, T.N. Review Processing, properties and applications of reactive silica from rice husk—An overview. *J. Mater. Sci.* **2003**, *38*, 3159–3168. [[CrossRef](#)]
9. Nair, D.G.; Fraaij, A.; Klaassen, A.A.; Kentgens, A.P. A structural investigation relating to the pozzolanic activity of rice husk ashes. *Cem. Concr. Res.* **2008**, *38*, 861–869. [[CrossRef](#)]
10. Rao, F.; Liu, Q. Geopolymerization and its potential application in mine tailings consolidation: A review. *Miner. Process. Extr. Metall. Rev.* **2015**, *36*, 399–409. [[CrossRef](#)]
11. Wang, K.; Du, L.; Lv, X.; He, Y.; Cui, X. Preparation of drying powder inorganic polymer cement based on alkali-activated slag technology. *Powder Technol.* **2017**, *312*, 204–209. [[CrossRef](#)]
12. Van, V.-T.-A.; Rößler, C.; Bui, D.-D.; Ludwig, H.-M. Rice husk ash as both pozzolanic admixture and internal curing agent in ultra-high performance concrete. *Cem. Concr. Compos.* **2014**, *53*, 270–278. [[CrossRef](#)]
13. Tuan, N.V.; Ye, G.; Breugel, K.B.; Copuroglu, O. Hydration and microstructure of ultra-high performance concrete incorporating rice husk ash. *Cem. Concr. Res.* **2011**, *41*, 1104–1111. [[CrossRef](#)]
14. Shi, C.; Wu, Z.; Xiao, J.; Wang, D.; Huang, Z.; Fang, Z. A review on ultra high performance concrete: Part I. Raw materials and mixture design. *Constr. Build. Mater.* **2015**, *101*, 741–751. [[CrossRef](#)]
15. Eisinias, A.; Baltakys, K.; Šiaučionas, R. The effect of gyrolite additive on the hydration properties of Portland cement. *Cem. Concr. Res.* **2012**, *42*, 27–38. [[CrossRef](#)]
16. Monteagudo, S.; Moragues, A.; Gálvez, J.C.; Casati, M.J.; Reyes, E. The degree of hydration assessment of blended cement pastes by differential thermal and thermogravimetric analysis. Morphological evolution of the solid phases. *Thermochim. Acta* **2014**, *592*, 37–51. [[CrossRef](#)]
17. Chen, W.; Li, Y.; Shen, P.; Shui, Z. Microstructural Development of Hydrating Portland Cement Paste at Early Ages Investigated with Non-destructive Methods and Numerical Simulation. *J. Nondestruct. Eval.* **2013**, *32*, 228–237. [[CrossRef](#)]

18. Ylmén, R.; Jäglid, U.; Steenari, B.-M.; Panas, I. Early hydration and setting of Portland cement monitored by IR, SEM and Vicat techniques. *Cem. Concr. Res.* **2009**, *39*, 433–439. [[CrossRef](#)]
19. Scrivener, K.L. Backscattered electron imaging of cementitious microstructures: Understanding and quantification. *Cem. Concr. Compos.* **2004**, *26*, 935–945. [[CrossRef](#)]
20. Zhang, J.; Lei, Q.; Li, Z. Hydration monitoring of cement-based materials with resistivity and ultrasonic methods. *Mater. Struct.* **2009**, *42*, 15–24. [[CrossRef](#)]
21. Xu, D.; Huang, S.; Qin, L.; Lu, L.; Cheng, X. Monitoring of cement hydration reaction process based on ultrasonic technique of piezoelectric composite transducer. *Constr. Build. Mater.* **2012**, *35*, 220–226.
22. Buttress, A.; Jones, A.; Kingman, S. Microwave processing of cement and concrete materials-towards an industrial reality? *Cem. Concr. Res.* **2015**, *68*, 112–123. [[CrossRef](#)]
23. Wang, H.; Gao, X.; Liu, J. Effects of salt freeze-thaw cycles and cyclic loading on the piezoresistive properties of carbon nanofibers mortar. *Constr. Build. Mater.* **2018**, *177*, 192–201. [[CrossRef](#)]
24. Materazzi, A.L.; Ubertini, F.; D’Alessandro, A. Carbon nanotube cement-based transducers for dynamic sensing of strain. *Cem. Concr. Compos.* **2013**, *37*, 2–11. [[CrossRef](#)]
25. Dong, S.; Han, B.; Ou, J.; Li, Z.; Han, L.; Yu, X. Electrically conductive behaviors and mechanisms of short-cut super-fine stainless wire reinforced reactive powder concrete. *Cem. Concr. Compos.* **2016**, *72*, 48–65. [[CrossRef](#)]
26. Shen, P.; Lu, L.; He, Y.; Wang, F.; Hu, S. Hydration monitoring and strength prediction of cement-based materials based on the dielectric properties. *Constr. Build. Mater.* **2016**, *126*, 179–189. [[CrossRef](#)]
27. Huang, H.; Gao, X.; Wang, H.; Ye, H. Influence of rice husk ash on strength and permeability of ultra-high performance concrete. *Constr. Build. Mater.* **2017**, *149*, 621–628. [[CrossRef](#)]
28. Wang, H.; Gao, X.; Wang, R. The influence of rheological parameters of cement paste on the dispersion of carbon nanofibers and self-sensing performance. *Constr. Build. Mater.* **2017**, *134*, 673–683. [[CrossRef](#)]
29. Cao, J.; Chung, D. Electric polarization and depolarization in cement-based materials, studied by apparent electrical resistance measurement. *Cem. Concr. Res.* **2004**, *34*, 481–485. [[CrossRef](#)]
30. Wen, S.; Chung, D. Electric polarization in carbon fiber-reinforced cement. *Cem. Concr. Res.* **2001**, *31*, 141–147. [[CrossRef](#)]
31. He, B.; Gao, Y.; Qu, L.; Duan, K.; Zhou, W.; Pei, G. Characteristics analysis of self-luminescent cement-based composite materials with self-cleaning effect. *J. Clean. Prod.* **2019**, *225*, 1169–1183. [[CrossRef](#)]
32. Gao, Y.; He, B.; Xiao, M.; Fang, Z.; Dai, K. Study on properties and mechanisms of luminescent cement-based pavement materials with super-hydrophobic function. *Constr. Build. Mater.* **2018**, *165*, 548–559. [[CrossRef](#)]
33. Gao, Y.; Qu, L.; He, B.; Dai, K.; Fang, Z.; Zhu, R. Study on effectiveness of anti-icing and deicing performance of super-hydrophobic asphalt concrete. *Constr. Build. Mater.* **2018**, *191*, 270–280. [[CrossRef](#)]
34. De Sensale, G.R.; Ribeiro, A.B.; Gonçalves, A. Effects of RHA on autogenous shrinkage of Portland cement pastes. *Cem. Concr. Compos.* **2008**, *30*, 892–897. [[CrossRef](#)]

